White Rose Research Online

eprints@whiterose.ac.uk
https://eprints.whiterose.ac.uk
Universities of Leeds, Sheffield and York

Deposited via The University of Sheffield.

White Rose Research Online URL for this paper:
https://eprints.whiterose.ac.uk/id/eprint/130799/

Version: Published Version

Article:
Balades, N., Sales, D.L., Herrera, M. et al. (2018) Analysis of Bi Distribution in Epitaxial GaAsBi by aberration-corrected HAADF-STEM. Nanoscale Research Letters, 13. 125. ISSN: 1931-7573

https://doi.org/10.1186/s11671-018-2530-5

© The Author(s). 2018 Open Access This article is distributed under the terms of the Creative Commons Attribution 4.0 International License (http://creativecommons.org/licenses/by/4.0/), which permits unrestricted use, distribution, and reproduction in any medium, provided you give appropriate credit to the original author(s) and the source, provide a link to the Creative Commons license, and indicate if changes were made.

Reuse
This article is distributed under the terms of the Creative Commons Attribution (CC BY) licence. This licence allows you to distribute, remix, tweak, and build upon the work, even commercially, as long as you credit the authors for the original work. More information and the full terms of the licence here: https://creativecommons.org/licenses/

Takedown
If you consider content in White Rose Research Online to be in breach of UK law, please notify us by emailing eprints@whiterose.ac.uk including the URL of the record and the reason for the withdrawal request.

UNIVERSITY OF LEEDS
University of Sheffield
UNIVERSITY of York

Baladés et al. Nanoscale Research Letters (2018) 13:125
https://doi.org/10.1186/s11671-018-2530-5

Nanoscale Research Letters

NANO EXPRESS Open Access

Analysis of Bi Distribution in Epitaxial GaAsBi by Aberration-Corrected HAADF-STEM

N. Baladés[1,2*], D. L. Sales[1,2], M. Herrera[1,2], C. H. Tan[3], Y. Liu[3], R. D. Richards[3] and S. I. Molina[1,2]

Abstract

The Bi content in GaAs/$GaAs_{1-x}Bi_x$/GaAs heterostructures grown by molecular beam epitaxy at a substrate temperature close to 340 °C is investigated by aberration-corrected high-angle annular dark-field techniques. The analysis at low magnification of high-angle annular dark-field scanning transmission electron microscopy images, corroborated by EDX analysis, revealed planar defect-free layers and a non-homogeneous Bi distribution at the interfaces and within the GaAsBi layer. At high magnification, the qHAADF analysis confirmed the inhomogeneous distribution and Bi segregation at the GaAsBi/GaAs interface at low Bi flux and distorted dumbbell shape in areas with higher Bi content. At higher Bi flux, the size of the Bi gathering increases leading to roughly equiaxial Bi-rich particles faceted along zinc blende {111} and uniformly dispersed around the matrix and interfaces. FFT analysis checks the coexistence of two phases in some clusters: a rhombohedral pure Bi (rh-Bi) one surrounded by a zinc blende $GaAs_{1-x}Bi_x$ matrix. Clusters may be affecting to the local lattice relaxation and leading to a partially relaxed GaAsBi/GaAs system, in good agreement with XRD analysis.

Keywords: GaAsBi, Ac-HAADF-STEM, Bi-clusters

Background

Nowadays, GaAsBi-based semiconductors are attracting interest as temperature-stable and mid-infrared devices [1]. Adding a small amount of Bi into the GaAs lattice leads to a large bandgap reduction, being one of the most interesting optoelectronic effects [2, 3]. However, incorporating even a small amount of Bi into GaAs is challenging due to the weak Ga–Bi bonding energy, the large miscibility gap and the large difference in the lattice constant between GaBi and GaAs. Consequently, GaAsBi has to be grown under a non-equilibrium dynamic process for an efficient Bi incorporation. Although even if it is synthesised successfully, the distribution of Bi is sometimes non-uniform, increasing the density of non-radiative recombination centres and therefore affecting their efficiency in lasing operation. The large size and low electronegativity of Bi tend to produce phase separation [4], surface droplets [5, 6], atomic ordering [7–9], nano-scale liquid droplets [10] or Bi clusters during epitaxial growth. The presence of Bi clusters was previously detected by Ciatto et al. through a combination of X-ray absorption spectroscopy (XAS), atomic force microscopy and X-ray diffraction (XRD) techniques [11]. Then, several authors reported the presence of Bi clusters in annealed GaAsBi samples by using different transmission electron microscopy techniques [4, 12, 13]. Furthermore, Kunzer et al. [14] confirmed by conventional electron spin resonance (ESR) that about 10% of the incorporated Bi had occupied the Ga sites in GaAsBi layers. Therefore, understanding and controlling the Bi incorporation and defect formation is critical for the successful application of GaAsBi to devices. It is worth mentioning that the development of new Bi-based materials is linked to the advancement of characterization tools. In this sense, high-angle annular dark-field scanning transmission electron microscopy (HAADF-STEM) techniques in aberration-corrected microscopes plays an important role in obtaining information at sub-angstrom level [15, 16]. In this technique, the intensity in the images is roughly proportional to the average atomic number

* Correspondence: nuria.balades@uca.es
[1]Department of Material Science, Metallurgical Engineering and Inorganic Chemistry, University of Cádiz, Campus Río San Pedro, 11510, Puerto Real, Cádiz, Spain
[2]Instituto Universitario de Investigación en Microscopía Electrónica y Materiales (IMEYMAT). Facultad de Ciencias. Universidad de Cádiz, Campus Río San Pedro s/n. 11510 Puerto Real, Cádiz, Spain
Full list of author information is available at the end of the article

Springer Open

© The Author(s). 2018 **Open Access** This article is distributed under the terms of the Creative Commons Attribution 4.0 International License (http://creativecommons.org/licenses/by/4.0/), which permits unrestricted use, distribution, and reproduction in any medium, provided you give appropriate credit to the original author(s) and the source, provide a link to the Creative Commons license, and indicate if changes were made.

(Z) in the projected atomic column, so it can be successfully applied in dilute Ga(AsBi) heterostructures due to the large difference in the atomic number of Bi with respect to As and Ga. In addition, bright features in HAADF images, contrary to the high-resolution transmission electron microscopy (HRTEM), can be associated to atomic columns in an aligned crystal due to the lack of contrast reversals and delocalization. Also, aberration-corrected HAADF images of GaAsBi samples show a low dependence on the specimen thickness and an almost linear dependence on the As/Bi composition [12]. Moreover, by applying the quantitative HAADF (qHAADF) image analysis algorithm, developed by Molina et al. [17], it is possible to correlate effectively HAADF intensity and atomic column composition in III–V ternary semiconductor materials [12, 16, 18] and consequently in GaAsBi compounds. Additionally, high-resolution HAADF-STEM images offer information about crystalline quality [19–22].

In this work, we investigate through aberration-corrected HAADF-STEM imaging and complementary energy-dispersive X-ray (EDX) the Bi distribution in $GaAs/GaAs_{1-x}Bi_x/GaAs$ heterostructures grown by molecular beam epitaxy (MBE) at a substrate temperature close to 340 °C. We also studied the effect of the Bi gathering at nano- and micro-scales. For this aim, we have used the qHAADF approach, the Fourier fast transform (FFT) analysis of high-resolution images and the XRD techniques.

Methods

We study a series of two samples consisting of $GaAs/GaAs_{1-x}Bi_x/GaAs$ heterostructures grown by solid source MBE on 2″ n^+ GaAs: Si (001) wafers with different Bi flux given by the Bi cell temperatures S1 (460 °C) and S2 (505 °C). The system used was a VG V80 MBE machine with an average resting background pressure of $\sim 5 \times 10^{-10}$ mbar. The structures nominally consist of a 130 nm GaAs buffer, 130 nm GaAsBi layer, 5 nm GaAs spacer layer and then a 130 nm GaAs cap. Prior to growth, the substrate was outgassed at 400 °C for 20 min and then the surface oxide was removed at 600 °C. The GaAs buffer and cap were grown at ~ 580 °C under an As_2 flux, while the GaAsBi layer and GaAs spacer layer were grown at ~ 340 °C under a near-stoichiometric As_4 flux. The GaAsBi layer was therefore annealed in situ at ~ 580 °C for ~ 20 min during the growth of the GaAs cap. Under these growth conditions, no metallic droplets at the surface were observed. The substrate temperatures were estimated using optical thermometry, with the results being calibrated against surface reconstruction transitions at known temperatures. Prior to GaAsBi growth, the sample surface was exposed to a Bi flux for 20 s; the purpose of this step was to establish a Bi surface layer and enhance Bi incorporation at the commencement of GaAsBi growth.

The specimens for HAADF-STEM were prepared in cross-section by mechanical grinding and Ar^+ ion milling using a precision ion polishing system (PIPS), with beam tilts of − 3° and + 4° and beam energy between 2.8 and 3.0 kV. At the final milling step, the ion energy was decreased to 1.5 kV to enhance surface quality. Samples before being studied were plasma-cleaned to reduce the effect of the electron beam deposition on the specimen surface [23]. HAADF-STEM images, zero-loss electron energy loss spectrum (EELS) and energy-dispersive X-ray spectra line scans were conducted at 200 kV, using a Titan^3 Themis at 60–300 kV. The Titan^3 Themis is equipped with a cold field emission gun (FEG), Cs probe corrector and electron monochromator, allowing atomic resolution in HAADF imaging. This microscope also includes a Super-X quad EDX detector for elemental analysis, providing information about atom position and composition simultaneously. Secondary electron (SE) images for the topography study of the TEM specimen were performed using a FEI NOVA NANOSEM 450 microscope at 2 kV.

The Bi-M line at 2.42 keV was used for the quantitative determination of Bi composition through the Bruker Espirit software. The thickness of the specimen was determined from the analysis of the spatially resolved zero-loss EELS signal, by using the Digital Micrograph (GATAN™) software [23]. The column-by-column Bi distribution has been studied using the qHAADF software available to run on the Digital Micrograph. This software allows measuring and mapping the integrated intensity of selected areas around atomic columns by detecting intensity peaks in the HAADF-STEM image [17]. The ω-2θ (0 0 4) XRD spectra were measured with a Bruker D8 Discover X-ray diffractometer using Cu-$K\alpha_1$ radiation. The scans were simulated using Bede Rads Mercury software.

Results and Discussion

Figure 1 shows low-magnification HAADF-STEM images taken on [110] zone axis of samples S1 (a) and S2 (b), together with the thickness gradient-corrected intensity profiles taken along the [001] direction from the regions marked in the HAADF-STEM images (green rectangles). No threading dislocations or stacking faults were detected in the studied regions of both samples. In HAADF, the intensity obtained is proportional to the average atomic number. So, for a constant sample thickness, the brighter contrast in the image is related to a higher Bi content ($Z_{Bi} = 83$, $Z_{Ga} = 31$ and $Z_{As} = 33$). This makes possible the study of the Bi distribution in GaAsBi/GaAs heterostructures. As it can be observed in

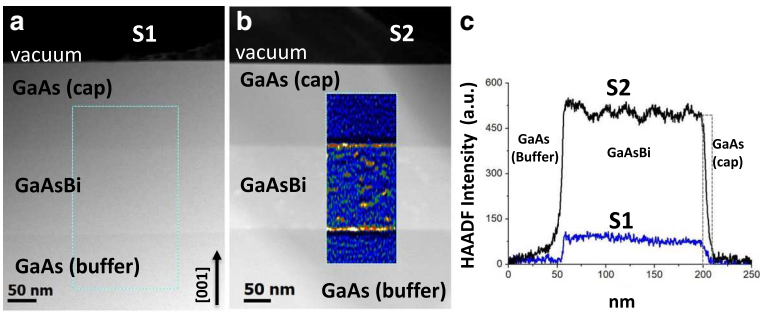

Fig. 1 **a** Cross-sectional HAADF-STEM images of sample S1 showing GaAs/GaAsBi/GaAs interfaces. **b** Cross-sectional HAADF-STEM image of sample S2, in the GaAsBi layer bright spots distributed along the GaAsBi layer related to Bi-rich areas are observed. Detail using temperature colour scale of an area after applying a low-pass filter is included as an inset in the same image for a better visualisation. **c** Thickness gradient-corrected intensity profiles taken along [001] direction from the regions marked with green rectangles in the HAADF-STEM images, blue line for sample S1 and black line for sample S2, showing a slightly different behaviour at the interfaces

Fig. 1a, no clear contrast variations are detected in the GaAsBi layer in sample S1—with a lower Bi content—not showing clear evidence of clustering, not even in other areas with higher sample thickness. However, Bi and As clusters have been reported in the literature, even for GaAsBi samples with Bi content as low as 1.44%, although grown at lower temperatures [11]. With regard to sample S2, with a higher Bi content, Fig. 1b depicts some areas with brighter contrast in the layer with a relatively homogeneous size and distribution. These regions, regularly distributed along the GaAsBi layer and interfaces, can be directly interpreted as Bi-containing clusters because of their higher HAADF intensity. For a better visualisation, the corresponding low-pass filtered image is shown as an inset in the same image, where the yellow colour corresponds to higher Bi content areas and the black to lower ones (temperature scale). The formation of Bi clusters in GaAsBi without provoking structural defects has been previously reported by other authors [7, 24, 25]. The integration of Bi (1.6 times the atomic volume of As) in the GaAs matrix may cause an increase in the substitutional energy because of the strain, reducing the solubility of the As atoms and allowing the gathering of the Bi ones. A study of the sample using a field emission gun scanning electron microscope (FEG-SEM) was performed to ensure that Bi clusters are embedded within the layer. For that purpose, topography images of secondary electrons acquired at low voltage (not shown here) were compared to STEM ones taken from the same area.

In order to obtain further information on the Bi distribution in the samples, intensity profiles along growth direction with corrected thickness gradient are shown in Fig. 1c. Profiles, taken from the HAADF-STEM images in Fig. 1a, b, point out a similar behaviour in both samples: roughly abrupt interfaces, GaAsBi layers of similar length (~ 140 nm). Regarding the GaAsBi/GaAs interface, the HAADF intensity drops from its maximum value to ~ 0 in about 10 nm (see the grey dashed rectangle in the profile), suggesting some Bi incorporation throughout the GaAs cap layer even without Bi flux. Profiles also depict information about equilibration time. As it can be observed from the profiles, in the lower Bi content sample (S1), the GaAs/GaAsBi interface is more abrupt than that in the higher Bi content sample (S2). This may be explained by the different Bi incorporation coefficients of the two samples. S1, while grown at the same temperature as S2, has a much smaller Bi content. S1 is therefore probably grown under kinetically limited conditions with near-unity Bi incorporation [26], meaning that the Bi surface layer will equilibrate over a time frame less than the surface lifetime of a Bi atom at this temperature. S2, on the other hand, probably has a lower Bi incorporation coefficient [27]. The Bi surface layer in this case would take more than the surface lifetime of a Bi atom to equilibrate, leading to a slower stabilisation of Bi incorporation.

To confirm the correlation made between the HAADF-STEM intensity profiles and the Bi distribution in the heterostructure, STEM-EDX Bi compositional maps of the samples were simultaneously taken. They are shown in Fig. 2 for sample at low (a) and high (b) Bi flux. The corresponding Bi compositional profiles along the growth direction, determined by integrating the point EDX spectra of an area of around 130 nm, are shown in Fig. 2c as blue and black lines respectively. These compositional profiles display the same tendency detected in the GaAs/GaAsBi/GaAs interfaces by low-magnification HAADF analysis. The average Bi atomic fraction in the GaAsBi layers was quantified from the corresponding EDX spectra being $1.2 \pm 0.4\%$ and $5.3 \pm 0.4\%$ in samples S1 and S2, respectively, showing a non-homogeneous distribution of Bi in the GaAsBi layer in both samples.

The presence of Bi clusters would be due to a steric hindrance effect. In this case, the surface tension may

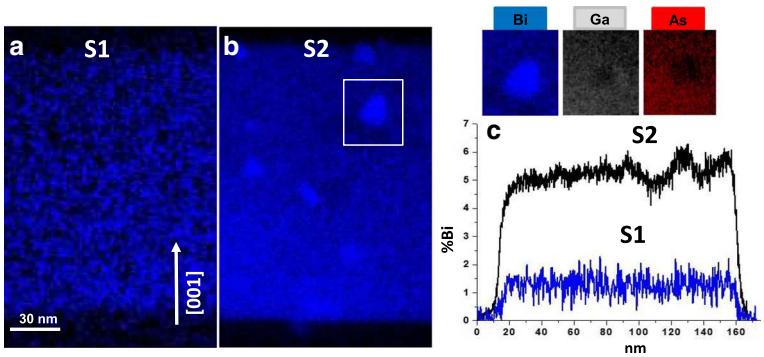

Fig. 2 STEM/EDX elemental maps representing Bi distribution in samples S1 (**a**) and S2 (**b**). Details of Bi, Ga and As elemental maps corresponding to the cluster marked with a white rectangle in Fig. 1b reveal a drop in As and Ga signals where there is a high Bi region. **c** Bi content profiles along [001] direction extracted after integration of an area of around 130 nm from the EDX map of samples S1 (blue line) and S2 (black line). Similar features were observed in the intensity profiles at low magnification shown in Fig. 1c

increase because of the larger atomic size of the Bi atoms, so to reduce the stress in the structure Bi atoms could be blocking Ga incorporation and consequently causing Ga vacancies in the net. Ga and As compositional maps of the cluster surrounded by a white square in Fig. 2b are included to show how both signals fall where there is a high Bi signal. This suggests that, in this particular cluster, Bi could be occupying both group III and group V sub-lattices. This also evidences that the clusters are not superficial ones formed during TEM sample preparation.

To carry out a deep study of the Bi distribution at the atomic level, high-magnification aberration-corrected HAADF-STEM images were taken in the [110] projection. In this III–V semiconductor alloy, the two maximum intensity peaks of a dumbbell correspond to group III and group V atomic columns. To properly correlate the intensity in the atomic columns with their composition, the background level has been removed from the experimental HAADF-STEM images. Then, an automatic location of the intensity peaks has been carried out, and integration areas around the group V atomic columns are carefully selected. Integrated intensities are measured and mapped for every dumbbell using the qHAADF approach. The procedure to quantify Bi content was similar to the one published in Ref. [28]. In this work, the integrated intensity quotients of every dumbbell (***R***) was calculated as a ratio between the integrated intensity in the group V columns (I_{As-Bi}) in the whole image and the mean integrated intensity in the group V columns in the GaAs layer (I_{As}), as $R = (I_{(As-Bi)})/I_{As}$.

Figure 3a shows a high-magnification HAADF-STEM image of the GaAs/GaAsBi interface taken from the sample with poor Bi content (S1). The coloured normalised integrated intensity map of the HAADF image is

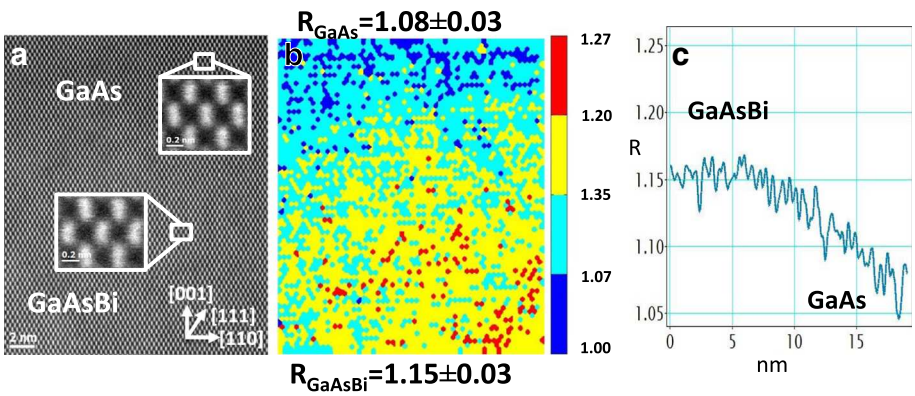

Fig. 3 a Cross-sectional [110] HAADF-STEM image of the interface GaAsBi/GaAs of sample S1. The detail of an undistorted region in the GaAs layer and distorted anion-cation dumbbells in a Bi-rich area at higher magnification are included as an inset in the same image. **b** Coloured map representing *R* values around group V columns of the HAADF image in Fig. 3a. The green colour corresponds to mean Bi composition in GaAsBi layer measured by EDX. Despite the homogeneous distribution of Bi in the HAADF-STEM image, the intensity map shows areas with high probability of nanoclustering (red dots) and columns with relative poor Bi content (blue dots) in the GaAsBi layer. **c** Profile along the growth direction of the whole *R* intensity map, showing a blurred GaAsBi/GaAs interface in about 10 nm

shown in Fig. 3b. Coloured dots ranging from 1 (deep blue) to 1.27 (red) depict the Bi content in the group V columns. As it can be observed, small fluctuations in *R* values from the mean value are found in both layers. In order to compare the dispersion of the obtained results, we have calculated the correlation coefficient ***Cv*** (defined as the ratio between the standard deviation and the mean *R* value) in the GaAs (substrate), the GaAsBi layer and the GaAs cap layer. The ***Cv*** values were 1.3, 2.6 and 2.6%, respectively, as fluctuations observed in GaAsBi/GaAs interface are higher than those found in the GaAs substrate taken as a reference; we can consider that these variations in *R* values are related to changes in Bi column composition. The cause of the non-zero ***Cv*** factor in the substrate may be due to local thickness fluctuations, detector noise (measured in a region without material as 0.6%) or hydrocarbons being deposited on the surface sample during microscopy characterisation.

This qHAADF analysis confirms a non-abrupt upper GaAsBi/GaAs interface over about 10 nm perceived at low magnification, mainly due to Bi surface segregation during growth, as it can be observed from the profile taken along the growth direction in the whole intensity *R* map, shown in Fig. 3c. Furthermore, dispersed Bi-rich columns within the GaAsBi layer (red dots), together with areas with a poor Bi content (blue dots) in the GaAsBi layer, are detected as well with this software, confirming the Bi content fluctuations in the GaAsBi layer. The presence of Bi-rich columns seems to be producing distinct distortion in the dumbbell shape as it can be appreciated in the inset at higher magnification in Fig. 3a. The substitution of As atoms for bigger Bi ones during the epitaxial growth would have locally broadened the lattice of the matrix, causing a distortion in the dumbbell shape while the structure is maintained.

HAADF-STEM techniques also enable structural and compositional analysis of the clusters detected at low magnification in sample S2. These clusters, almost homogeneously distributed, occupy around 20–30% of the GaAsBi layer surface. To know Bi composition, shape and size of the clusters found, aberration-corrected HAADF-STEM images were taken in the [110] projection and EDX elemental maps and intensity map ratios around group V columns were performed. To identify different crystalline phases, a fast Fourier transform (FFT) study was carried out in the high-resolution images in different areas inside and nearby the clusters.

Figure 4a shows a high-resolution [110] HAADF-STEM image of the GaAsBi/GaAs interface with a clear Bi cluster of about 12 nm diameter. Red rectangles in the image represent the areas where the FFT study was performed. It is well known that low-pass filtering not

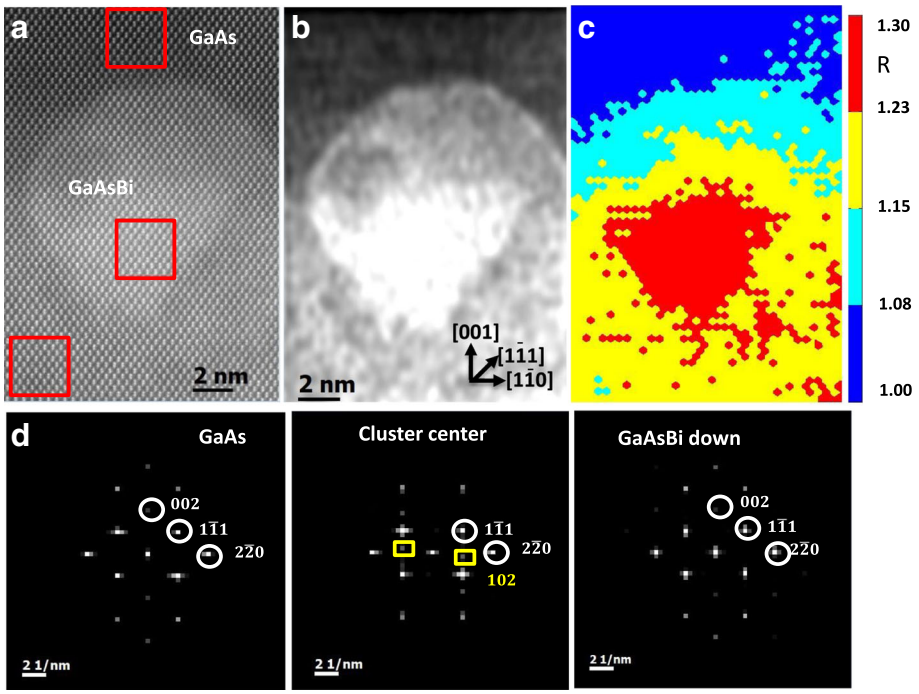

Fig. 4 a Cross-sectional [110] HAADF-STEM image of the interface GaAsBi/GaAs of sample S2, capturing a Bi cluster of about 12 nm in size, next to the GaAsBi/GaAs interface. **b** Low-filtered image of the HAADF-STEM image shows two areas with different contrast in the GaAsBi layer, a Bi-rich zone is faceted along {111} and (001) planes, surrounded by a lower Bi-rich one. **c** Coloured map representing the *R* values around group V columns depicting a graded Bi distribution around the cluster. **d** The corresponding Fourier transformation from the selected areas marked with red rectangles in Fig. 1a. Additional spots matching {102} planes related to rh-Bi phase are detected in the highest contrast cluster region

only reduces the amount of noise in the data, but it also removes the periodic features observed in the raw image, emphasising the edges of the Bi cluster. The filtered HAADF-STEM image, following the procedure described by Werner et al. [29], is shown in Fig. 4b. As it can be appreciated, {111} and (001) facets in the brightest area are clearly observable. However, the intensity distribution suggests the presence of two different compositional volumes in the particle: a Bi-rich one with trapezoidal shape surrounded by a less Bi-rich area. A similar cluster shape was observed for Wood et al. in a five-period $GaAs_{1-x}Bi_x/GaAs_{1-y}Bi_y$ structure [10].

The qHAADF analysis through the intensity ***R*** map shown in Fig. 4c depicts a roughly equiaxial particle shape and a Bi concentration gradient peaked at the centre of the cluster.

Wu et al. [4] reported the presence of different crystallographic structures in GaAsBi layers studying HRTEM micrographs and modelling the formation and the phase transformation from zinc blende Bi-rich to rhombohedral Bi (rh-Bi) nucleated in zinc blende {111} planes. In this sense, it is worth mentioning that bright spots in the FFT from high-resolution HAADF-STEM images can be interpreted as diffraction spots from crystallographic planes. Then, extra spots in the conventional pattern for the zinc blende structure of GaAs should be interpreted as additional phases. To study the presence of different crystal structures in the cluster, Fig. 4d shows the FFTs corresponding to three different areas marked as red squares in Fig. 1a. From right to left shows a homogeneous region in GaAs cap layer, the brightest zone in the GaAsBi layer and another region with lower contrast in the same GaAsBi layer. White circles denote the position of diffraction peak with Miller indices 002, $1\bar{1}1$ and $2\bar{2}0$. As it can be observed, only in the centre of the cluster appears clear spots, marked with a yellow square, related to {102} planes roughly parallel to zinc blende {220} planes, suggesting that a new rh-Bi phase has nucleated in the GaAsBi zinc blende layer. FFTs also depict a broadening of the diffraction peaks related to {111} planes. This observed asymmetric peak may be due to the micro-strain causes by shearing {111} planes between rh-Bi and zinc blende phases in the cluster.

For a deep study of cluster composition, it is worth mentioning that when electrons go through an electron transparent specimen with embedded clusters, they carry information not only about the cluster, but also from the matrix. So, to estimate real cluster composition, we follow the same procedure described in Ref. [25]. Results also pointed out that clusters close to the GaAsBi/GaAs interface tend to be smaller in size (12 nm) with a higher Bi content (≈ 30%), probably due to the presence of Bi on the surface when the cap layer begins to be grown. However, most of the clusters located inside the GaAsBi layers have a bigger size (16 nm), but their Bi content is inferior (≈ 22%). Additionally, in the GaAsBi layer, clusters with superior Bi content (35%) and higher size (23 nm) were detected. Additionally, as it was mentioned before, the core of some clusters consist of pure rh-Bi.

In order to investigate the strain state of the epitaxial film, high-resolution X-ray ω-2θ curves were recorded. Figure 5 shows the (004) XRD scans of the GaAsBi/GaAs layers in blue and simulated fits in orange for samples S1 (a) and S2 (b). In both samples, the sharpest and highest intensity peak located at 0° arc seconds corresponds to the GaAs substrate, while the broad lower intensity peak located at negative arc seconds corresponds to the strained GaAsBi layer. The angle between the peaks relates to the amount of lattice mismatch between both layers. The shoulder to the right of the GaAs peak in the spectrum of S2 indicates a GaAs layer under tensile strain; this implies strain relaxation in the S2 GaAsBi layer. The XRD spectrum of sample S1 was well fitted using the Bi fraction and thicknesses given by the EDX and HAADF measurements. There is no indication

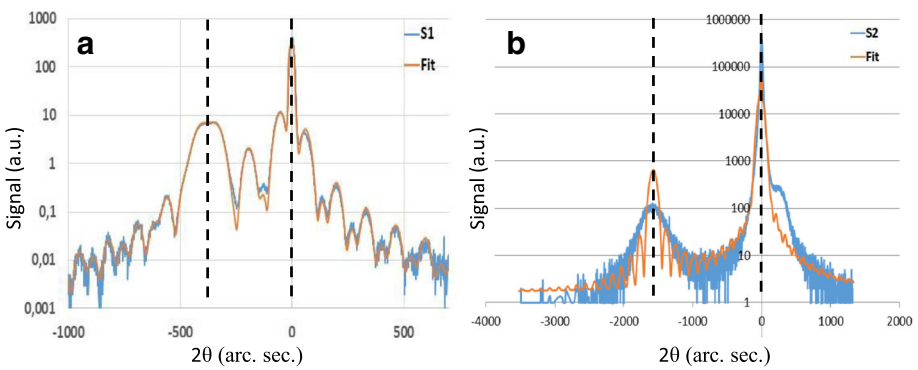

Fig. 5 X-ray diffraction data (blue lines) and simulated fits (orange lines) of sample S1 (**a**) and sample S2 (**b**). Vertical dashed lines highlighting the GaAs peak at 0° arc seconds and the GaAsBi film peak located at negative arc seconds. The shoulder on the right GaAs peak in Fig. 5b is indicative of a GaAs cap layer under tensile strain

of any strain relaxation in the XRD spectrum of sample S1. The XRD spectrum of sample S2 was more problematic to fit. Figure 5b shows the data modelled by a uniform GaAsBi layer of 5.8%, as determined by the HAADF-STEM analysis, ignoring the Bi rich clusters, and a relaxation of the GaAsBi layer of 6%, as determined by fitting the XRD curve; this would be reasonable if the clusters were not coherent with the rest of the GaAsBi matrix. This model does not accurately represent the layer; while the substrate-GaAsBi splitting is sufficient to account for the data, no tensile GaAs peak at ~ 250° arc seconds is visible. The tensile GaAs peak suggests that relaxation has occurred within the layer. Relaxation of a compressive layer will reduce the out of plane lattice constant, which implies that the modelled average Bi content of 5.8% is an underestimate of the real average; this is consistent with the observation of Bi-rich clusters in the layer. No peak(s) corresponding to ~ 22–35% GaAsBi was observed by reciprocal space mapping (not shown), which suggests that the clusters may not be coherent with the GaAsBi matrix. No further modelling of the S2 XRD spectrum was attempted.

Conclusions

The ac-HAADF-STEM analyses offer useful information about structure and composition of GaAs/GaAsBi/GaAs heterostructures, the results being in good agreement with EDX, FFT and XRD investigations. The analysis of low-magnification HAADF-STEM images allowed detecting inhomogeneous Bi distribution and non-abrupt GaAsBi/GaAs interfaces. At high magnification, the qHAADF analysis revealed clear Bi segregation at the GaAsBi/GaAs interface at low Bi flux (S1), and distorted dumbbell shape in areas with higher Bi fraction, due to As-substitutional positions of Bi atoms in the group V subnet. At higher Bi flux (S2), the size of the Bi gathering raises leading to roughly equiaxial clusters uniformly dispersed around the whole matrix and interfaces. The study revealed the coexistence of two different crystalline phases in the studied clusters rh-Bi and zinc blende shearing {111} planes, affecting to the local lattice relaxation and leading to a partially relaxed GaAsBi/GaAs system, in good agreement with XRD analysis.

Abbreviations

Ac-HAADF-STEM: Aberration-corrected high-angle annular dark-field scanning transmission electron microscopy; EDX: Energy-dispersive X-ray; EELS: Electron energy loss spectrum; ESR: Conventional electron spin resonance; FEG: Cold field emission gun; FFT: Fourier fast transform; HRTEM: High-resolution transmission electron microscopy; IMEYMAT: Instituto Universitario de Investigación en Microscopía Electrónica y Materiales; MBE: Molecular beam epitaxy; qHAADF: Quantitative HAADF image analysis algorithm; SEM: Scanning electron microscope; XAS: X-ray absorption spectroscopy; XRD: X-ray diffraction

Acknowledgements

We acknowledge F.J. Delgado for helping with the TEM specimen preparation and DME-SCICyT-UCA facilities.

Funding

This work was supported by the Spanish MINECO (project TEC2014-53727-C2-2-R), Junta de Andalucía (PAI research group TEP-946) and European Union H2020 Program (PROMIS ITN European network). The work of R. D. Richards was funded in part by the EPSRC Doctoral Prize Fellowship scheme and in part by the Royal Academy of Engineering under the Research Fellowships scheme.

Availability of Data and Materials

The data and materials are deposited at the University of Cádiz and the University of Sheffield. They could be made available to the interested party under a motivated request addressed to the corresponding author.

Authors' Contributions

SIM proposed this work. CHT and RDR grew the heterostructure. CHT, RDR and YL performed the XRD analysis. NB collaborated in the TEM sample preparation. NB and DLS designed the STEM experiment and performed the STEM data acquisition. NB carried out the HAADF-STEM measurements, conducted the data analysis and wrote the first draft of the manuscript under the supervision of MH and DLS. All authors discussed the results and subsequently participated in the revision and approval of the final version of the manuscript.

Competing Interests

The authors declare that they have no competing interests.

Publisher's Note

Springer Nature remains neutral with regard to jurisdictional claims in published maps and institutional affiliations.

Author details

[1]Department of Material Science, Metallurgical Engineering and Inorganic Chemistry, University of Cádiz, Campus Río San Pedro, 11510, Puerto Real, Cádiz, Spain. [2]Instituto Universitario de Investigación en Microscopía Electrónica y Materiales (IMEYMAT). Facultad de Ciencias. Universidad de Cádiz, Campus Río San Pedro s/n. 11510 Puerto Real, Cádiz, Spain. [3]Department of Electronic and Electrical Engineering, University of Sheffield, S3 7HQ, Sheffield, UK.

Received: 28 November 2017 Accepted: 16 April 2018
Published online: 25 April 2018

References

1. Hunter CJ, Bastiman F, Mohmad AR, Richards R, Ng JS, Sweeney SJ, David JPR (2012) Absorption characteristics of $GaAs_{1-x}Bi_x$/GaAs diodes in the near-infrared. Ieee Photonic Tech L 24:2191–2194
2. Francoeur S, Seong MJ, Mascarenhas A, Tixier S, Adamcyk M, Tiedje T (2003) Band gap of $GaAs_{1-x}Bi_x$, $0 < x < 3.6\%$. Appl Phys Lett 82:3874–3876
3. Tixier S, Adamcyk M, Tiedje T, Francoeur S, Mascarenhas A, Wei P, Schiettekatte F (2003) Molecular beam epitaxy growth of $GaAs_{1-x}Bi_x$. Appl Phys Lett 82:2245–2247
4. Wu MJ, Luna E, Puustinen J, Guina M, Trampert A (2014) Formation and phase transformation of Bi-containing QD-like clusters in annealed GaAsBi. Nanotechnology 25(20):205605
5. Sterzer E, Knaub N, Ludewig P, Straubinger R, Beyer A, Volz K (2014) Investigation of the microstructure of metallic droplets on Ga(AsBi)/GaAs. J Cryst Growth 408:71–77
6. Tait CR, Yan LF, Millunchick JM (2017) Droplet induced compositional inhomogeneities in GaAsBi. Appl Phys Lett 111(4):042105
7. Norman AG, France R, Ptak AJ (2011) Atomic ordering and phase separation in MBE $GaAs_{(1-x)}Bi_{(x)}$. J Vac Sci Technol B 29(3):03C121
8. Reyes DF, Bastiman F, Hunter CJ, Sales DL, Sanchez AM, David JPR, Gonzalez D (2014) Bismuth incorporation and the role of ordering in GaAsBi/GaAs structures. Nanoscale Res Lett 9:23
9. Beyer A, Knaub N, Rosenow P, Jandieri K, Ludewig P, Bannow L, Koch SW, Tonner R, Volz K (2017) Local bi ordering in MOVPE grown Ga(As, Bi) investigated by high resolution scanning transmission electron microscopy. Applied Materials Today 6:22–28

10. Wood AW, Chen WX, Kim H, Guan YX, Forghani K, Anand A, Kuech TF, Mawst LJ, Babcock SE (2017) Annealing-induced precipitate formation behavior in MOVPE-grown $GaAs_{1-x}Bi_x$ explored by atom probe tomography and HAADF-STEM. Nanotechnology 28(21):215704
11. Puustinen J, Wu M, Luna E, Schramm A, Laukkanen P, Laitinen M, Sajavaara T, Guina M (2013) Variation of lattice constant and cluster formation in GaAsBi. J Appl Phys 114(24):243504
12. Sales DL, Guerrero E, Rodrigo JF, Galindo PL, Yanez A, Shafi M, Khatab A, Mari RH, Henini M, Novikov S, Chisholm MF, Molina SI (2011) Distribution of bismuth atoms in epitaxial GaAsBi. Appl Phys Lett 98:101902
13. Butkute R, Niaura G, Pozingyte E, Cechavicius B, Selskis A, Skapas M, Karpus V, Krotkus A (2017) Bismuth quantum dots in annealed GaAsBi/AlAs quantum wells. Nanoscale Res Lett 12:436
14. Kunzer M, Jost W, Kaufmann U, Hobgood HM, Thomas RN (1993) Identification of the BiGa heterosite defect in GaAs-Bi. Phys Rev B 48:4437–4441
15. Kret S, Ruterana P, Rosenauer A, Gerthsen D (2001) Extracting quantitative information from high resolution electron microscopy. Physica Status Solidi B-Basic Research 227:247–295
16. Grieb T, Müller K, Fritz R, Schowalter M, Neugebohrn N, Knaub N, Volz K, Rosenauer A (2012) Determination of the chemical composition of GaNAs using STEM HAADF imaging and STEM strain state analysis. Ultramicroscopy 117:15–23
17. S.I. Molina, D.L. Sales, P.L. Galindo, D. Fuster, Y. Gonzalez, B. Alen, L. Gonzalez, M. Varela, S.J. Pennycook, Column-by-column compositional mapping by Z-contrast imaging (vol 109, pg 172, 2009), Ultramicroscopy, 109 (2009) 1315–1315
18. Molina SI, Guerrero MP, Galindo PL, Sales DL, Varela M, Pennycook SJ (2011) Calculation of integrated intensities in aberration-corrected Z-contrast images. J Electron Microsc 60:29–33
19. Akamine H, van den Bos KHW, Gauquelin N, Farjami S, Van Aert S, Schryvers D, Nishida M (2015) Determination of the atomic width of an APB in ordered CoPt using quantified HAADF-STEM. J Alloy Compd 644:570–574
20. Grillo V, Rossi F (2011) A new insight on crystalline strain and defect features by STEM-ADF imaging. J Cryst Growth 318:1151–1156
21. Pyrz WD, Blom DA, Sadakane M, Kodato K, Ueda W, Vogt T, Buttrey DJ (2010) Atomic-level imaging of Mo-V-O complex oxide phase intergrowth, grain boundaries, and defects using HAADF-STEM. P Natl Acad Sci USA 107:6152–6157
22. Azough F, Freer R, Schaffer B (2010) Direct observation of A-site vacancies and a twin boundary structure in $La_{2/3}TiO_3$-based ceramics using HAADF/STEM. J Am Ceram Soc 93:1237–1240
23. Egerton RF, Li P, Malac M (2004) Radiation damage in the TEM and SEM. Micron 35:399–409
24. Norman AG, Seong TY, Ferguson IT, Booker GR, Joyce BA (1993) Structural studies of natural superlatticesin group III-V alloy epitaxial layers. Semicond Sci Tech 8:S9–S15
25. Dominguez L, Reyes DF, Bastiman F, Sales DL, Richards RD, Mendes D, David JPR, Gonzalez D (2013) Formation of tetragonal InBi clusters in InAsBi/InAs(100) heterostructures grown by molecular beam epitaxy. Appl Phys Express 6(11): 112601
26. Ptak AJ, France R, Beaton DA, Alberi K, Simon J, Mascarenhas A, Jiang CS (2012) Kinetically limited growth of GaAsBi by molecular-beam epitaxy. J Cryst Growth 338:107–110
27. Richards RD, Bastiman F, Hunter CJ, Mendes DF, Mohmad AR, Roberts JS, David JPR (2014) Molecular beam epitaxy growth of GaAsBi using As-2 and As-4. J Cryst Growth 390:120–124
28. Hernandez-Maldonado D, Herrera M, Alonso-Gonzalez P, Gonzalez Y, Gonzalez L, Gazquez J, Varela M, Pennycook SJ, Guerrero-Lebrero MD, Pizarro J, Galindo PL, Molina SI (2011) Compositional analysis with atomic column spatial resolution by 5th-order aberration-corrected scanning transmission electron microscopy. Microsc Microanal 17:578–581
29. Werner K, Beyer A, Oelerich JO, Baranovskii SD, Stolz W, Volz K (2014) Structural characteristics of gallium metal deposited on Si (001) by MOCVD. J Cryst Growth 405:102–109

Submit your manuscript to a SpringerOpen journal and benefit from:

- ► Convenient online submission
- ► Rigorous peer review
- ► Open access: articles freely available online
- ► High visibility within the field
- ► Retaining the copyright to your article

Submit your next manuscript at ► springeropen.com